1 **Drought shifts sorghum root metabolite and microbiome profiles and enriches**

2 **the stress response factor pipecolic acid**

3 Running title: Bacterial and Metabolite Profiling of Sorghum Roots

4

5 Daniel F. Caddell[1,2], Katherine Louie[3,4], Benjamin Bowen[3,4], Julie A. Sievert[5], Joy

6 Hollingsworth[5], Jeffery Dahlberg[5], Elizabeth Purdom[6], Trent Northen[3,4], Devin Coleman-

7 Derr[1,2#]

8

9 [1]Plant Gene Expression Center, USDA-ARS, Albany, CA 94710, USA

10 [2]Plant and Microbial Biology Department, UC Berkeley, Berkeley, CA 94720, USA

11 [3]Lawrence Berkeley National Laboratory, Berkeley, CA 94720, USA

12 [4]Joint Genome Institute, Berkeley, CA 94720, USA

13 [5]Kearney Agricultural Research & Extension Center, Parlier, CA 93648, USA

14 [6]Department of Statistics, UC Berkeley, Berkeley, CA 94720, USA

15 [#]Corresponding author: D.Coleman-Derr; E-mail: colemanderr@berkeley.edu

16

17 Word count: Abstract- 250 / Main Text- 3,918

18

19 **Keywords**: drought, roots, 16S rRNA, amplicon sequencing, microbiome,

20 metabolomics, pipecolic acid, sorghum

21

ABSTRACT

Interactions between plants and their root-associated microbiome are important for determining host fitness during periods of stress. During drought, monoderm bacteria are more abundant in sorghum roots than in those of watered controls. Additionally, a reversion from monoderm to diderm dominance occurs in drought-stressed roots one week after rewatering. However, the mechanisms driving this rapid microbiome composition shift is currently unknown. To understand if changes in host metabolism are correlated with this shift, we employed 16S amplicon sequencing and metabolomics of root, rhizosphere, and soil at the peak of a preflowering drought and 24 hours after rewatering. The microbiomes of droughted roots, rhizospheres, and soils differed from watered controls, and shifts in bacterial composition were observed in root and rhizosphere 24 hours after rewatering, highlighting the rapid response of microbes to the cessation of drought. Next, we performed metabolomic profiling to identify putative drivers of this process. During drought, we observed a high abundance of abiotic stress response factors, including antioxidants, osmolytes, amino acids, and plant hormones. After rewatering, large shifts in metabolite abundances were observed in rhizosphere, whereas shifts in root and soil were subtle. In addition, pipecolic acid, a well-characterized systemic acquired resistance signalling compound, was enriched in roots and rhizosphere during drought. We found that exogenous application of pipecolic acid suppresses root growth via a systemic acquired resistance-independent mechanism. Collectively, these data provide a comprehensive characterization of metabolite shifts across three compartments during drought, and elucidate a potential role of pipecolic acid in the sorghum drought response.

47

IMPORTANCE

Plant-associated microbial communities shift in composition and contribute to host

fitness during drought. In particular, Actinobacteria are enriched in plant roots and

rhizosphere during drought. However, the mechanisms plants use to drive this shift are

poorly understood. Here we apply a combination of bacterial and metabolite profiling in

root, rhizosphere, and soil during drought and drought-recovery to investigate potential

contributions of host metabolism towards shifts in bacterial composition. Our results

demonstrate that drought alters metabolic profiles and that the response to rewatering

differs between compartments; we identify drought-responsive metabolites that are

highly correlated with Actinobacteria abundance. Furthermore, our study reports for the

first time that pipecolic acid is a drought-enriched metabolite in sorghum roots. We

demonstrate that exogenous application of pipecolic acid is able to provoke one of the

classic drought responses in roots, root growth suppression, and that this activity

functions independently from the systemic acquired resistance pathway.

62

INTRODUCTION

Drought is one of the most significant abiotic stresses impacting agricultural production

and threatens to become an even bigger concern due to climate change. Root-

associated microbial communities, commonly referred to as microbiomes, influence

plant responses to a wide-variety of environmental stresses including drought, and are

capable of promoting improved fitness (1). In order to engineer microbiomes capable of

enhancing plant growth and ameliorating stress, more research is needed to understand

70 what signals plants use to simultaneously recruit beneficial microbes, while repelling

71 potential pathogens, from a broad pool of soil microbes. Taking advantage of advances

72 in high-throughput sequencing technologies, researchers are beginning to understand

73 the dynamic nature of the microbiome and its association with plant roots. For instance,

74 it is now known that microbiomes vary between environments (2–4), between species

75 (5–7), and even varieties of the same species (4, 8–10). Additionally, microbiomes are

76 dynamic and shift with developmental age, particularly as the plant transitions between

77 vegetative and reproductive growth (11–13). The root microbiome also responds to

78 abiotic stresses. For example, enrichment of monoderm bacteria, such as

79 Actinobacteria, during drought has been observed across diverse plant clades (6, 7, 13,

80 14). Notably, recent studies have demonstrated that plants mediate the shifts in

81 bacterial communities during drought (15), and Actinobacterial enrichment during

82 drought is dependent on signals produced by living roots (16). While monoderm

83 bacteria are dominant during drought, their enrichment is transitory, with diderm

84 bacteria reestablishing after rewatering (13). Despite their significance, the dynamics

85 regulating monoderm enrichment during drought and the subsequent shift to diderm

86 dominance after rewatering is not yet understood.

87

88 Plant-derived metabolites are predicted to drive some of the changes in the root

89 microbiome, as exudation patterns between photoperiods (17) and across development

90 (11, 18, 19) both track with changes in the microbiome. Additionally, a recent study of

91 the maize leaf microbiome across 300 maize genotypes observed associations between

92 specific microbial taxa and host metabolic functions (20). Different combinations of root

4

93 exudates are sufficient to alter microbiome composition (21), likely by impacting

94 attraction and behavior of soil microbes (22, 23). Some root exudates can act as carbon

95 sources for microbes, while others simultaneously promote certain microbial taxa and

96 suppress others (24). Exudation of putative defense-related metabolites, including

97 organic acids, may also act to repel microbes (23, 25–29). Drought promotes changes

98 in exudate composition, stimulating the exudation of primary and secondary

99 metabolites, including osmoprotectants such as sugars and amino acids. These root

100 and rhizosphere metabolites are predicted to play a role in regulating microbiome

101 associations during drought (30, 31).

102

103 Abiotic stresses also contribute to the modulation of plant immunity through

104 modifications to the balance of many hormone pathways, including abscisic acid (ABA),

105 salicylic acid (SA), jasmonic acid (JA), and ethylene (32). For example, ABA, which is

106 strongly induced by drought, antagonizes systemic acquired resistance (SAR) both

107 upstream and downstream of SA (33). In sorghum (*Sorghum bicolor* (L.) Moench),

108 reduced expression of both SA and JA-responsive genes occurs during a prolonged

109 drought (34). This phenomenon has also been observed in response to other abiotic

110 stresses as well; sorghum has reduced SA biosynthesis during nitrogen-limiting

111 conditions (35), and *Arabidopsis* represses immune signalling genes in response to

112 phosphate stress (36). This modulation has major implications for plant-associated

113 microbiomes, as microbes that colonize plant roots must either evade or suppress host

114 immune responses in order to thrive; mutants deficient in immune activation (37) and

115 exogenous application of plant defense hormones JA (38, 39) and SA (40) are both

5

116   sufficient to alter root microbiomes. Collectively, these studies support the hypothesis

117   that the plant immune system is in part responsible for regulating the establishment of

118   the root microbiome and is impacted by abiotic stress.
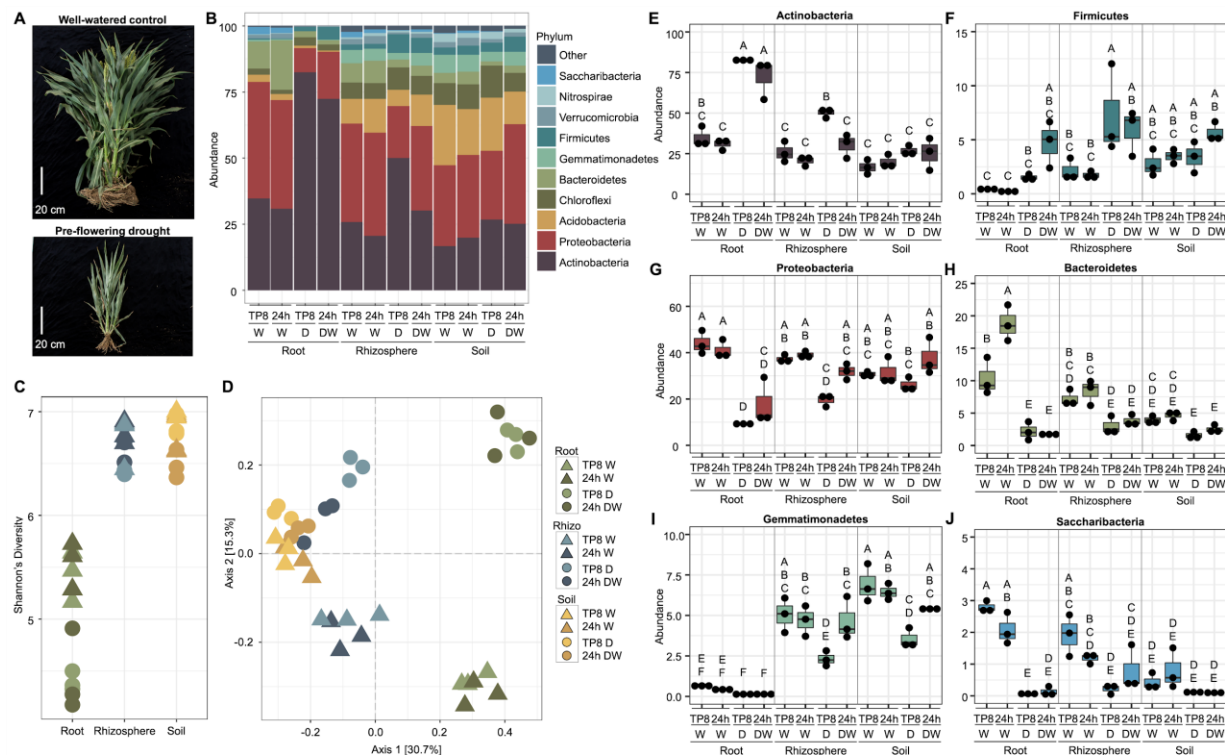
119

120   In this study, we utilize preflowering drought in field grown sorghum to determine if host

121   metabolism drives the enrichment of monoderm bacteria during drought, and whether

122   drought-driven changes in metabolites may play a role in the rapid transition from

123   monoderm to diderm dominance during re-acclimation to watering. Towards this goal,

124   we employed 16S amplicon sequencing and metabolomic profiling of root, rhizosphere,

125   and soil at the peak of drought and 24 hours after rewatering. We observe an

126   enrichment of monoderm bacteria during drought, consistent with previous reports (6, 7,

127   13). Furthermore, we determine that the microbiome responds rapidly to rewatering,

128   particularly in the rhizosphere. We also discover that drought alters the metabolite

129   profiles of sorghum root, rhizosphere, and soil. In particular, known drought-associated

130   metabolites such as betaine, 4-aminobutanoic acid (GABA), and amino acids including

131   proline are enriched during drought. Notably, the abundance of a large number of

132   rhizosphere metabolites are rapidly depleted by rewatering following drought, whereas

133   few metabolites shift abundance in the root. In addition to known drought-associated

134   metabolites, we report the detection of pipecolic acid (Pip), a lysine catabolite that is an

135   essential component of SAR (41, 42), as a drought-enriched metabolite in sorghum.

136   Here, we demonstrate that exogenous application of Pip suppresses plant root growth,

137   and that this activity functions independently from the established SAR pathway.

138

139 **RESULTS**

140 **The sorghum root-associated microbiome is influenced by drought and responds**

141 **rapidly to rewatering**

142 To examine the effect of a prolonged drought on the root microbiome of sorghum, a field

143 experiment was performed at the University of California's Agriculture and Natural (UC-

144 ANR) Resources Kearney Agricultural Research and Extension (KARE) Center, in

145 which sorghum plants were subjected to a prolonged preflowering drought, where no

146 water was applied between planting and the onset of flowering (TP8), or regularly

147 irrigated throughout the experiment (figure 1a). We performed 16S rRNA community

148 profiling of root, rhizosphere, and soil using Illumina MiSeq, targeting the V3-V4 variable

149 regions (figure 1b-j). In agreement with a previous study of the sorghum drought

150 microbiome, which was performed at the same location (13), alpha diversity significantly

151 differed between sample types (Shannon, $F=82.19$, $P=1.36\times10^{-13}$), with lower diversity

152 in the root, as compared with rhizosphere and soil, and reduced diversity in droughted

153 roots compared with watered roots (ANOVA, Tukey-HSD, $P<0.001$) (figure 1c). Beta

154 diversity was assessed through principal coordinates analysis (PCoA) using Bray–Curtis

155 dissimilarities. The primary axis distinguished samples foremost by compartment (root,

156 rhizosphere, or soil), and the second axis by watering regime (droughted or well-

157 watered) (figure 1d), suggesting that both compartment and drought were major driving

158 factors in shaping the microbiome. Pairwise permutational multivariate analysis of

159 variance (PERMANOVA) was performed for each compartment, treatment, and the

160 interaction between compartment and treatment, and all were significantly different

161 ($q<0.05$) (figure 1d).

7

162

163 Similar to previous studies of root microbiomes, we observed a significant enrichment of

164 monoderm bacteria during drought, including taxa belonging to the phylum

165 Actinobacteria in root and rhizosphere, and Firmicutes in the rhizosphere (ANOVA,

166 Tukey-HSD, P<0.05) (figure 1b,e-f). Likewise, diderm lineages were depleted during

167 drought, including Proteobacteria in roots and rhizosphere, Bacteroidetes in roots, and

168 Gemmatimonadetes in the rhizosphere (ANOVA, Tukey-HSD, P<0.05) (figure 1b,g-i).

169 These results suggest that the sorghum root-associated microbiome was responsive to

170 drought, in corroboration with past studies.

171

172

173

174   ***Figure 1. Sorghum root-associated microbiome responds to drought and***

175   ***rewatering. A*** *Representative image of sorghum plants following eight weeks of a*

176   *preflowering drought (TP8).* ***B*** *Phylum level relative abundances of sorghum root,*

177   *rhizosphere, and soil microbiomes at TP8 and 24 hours after rewatering (24h DW) in*

178   *well-watered (W) or drought (D) plots.* ***C*** *Alpha diversity (Shannon) of sorghum root,*

179   *rhizosphere, and soil.* ***D*** *Beta diversity (PCoA) of sorghum root, rhizosphere, and soil*

180   *microbiomes at TP8 and 24 hours after rewatering in well-watered control or drought*

181   *plots.* ***E-J*** *Relative abundances of individual lineages that displayed a significant*

182   *difference in abundance between watering treatments* (ANOVA, Tukey-HSD, P<0.05)*.*

183

184   Following drought, the sorghum root microbiome responds dramatically to rewatering,

185   with a transition from monoderm back to diderm dominance after a one week recovery

186   period (13). To better understand the early dynamics of this response to rewatering, we

187   watered the droughted sorghum plots after sampling at TP8, and another sampling was

188   performed 24 hours later. Notably, no significant shifts in relative abundance of root

189   phyla were observed (figure 1b). However, a depletion in Actinobacteria and an

190   increase in Gemmatimonadetes occurred in the rhizosphere (ANOVA, Tukey-HSD,

191   P<0.05) (figure 1b,e,i), consistent with monoderm to diderm transitions previously

192   observed after one week of drought recovery (13). Based on levels of beta diversity, the

193   rewatered rhizosphere microbiome appeared more similar to soil, rather than

194   rhizosphere from control samples (figure 1d). These results suggest that the

195   rhizosphere environment provokes a more rapid return to diderm dominance than the

196   root upon rewatering.

197

Drought alters the metabolite profiles of sorghum root, rhizosphere, and soil

199   Recently, substrate utilization was determined to drive microbe community assembly in

200   the rhizosphere across developmental age in another member of the grass lineage,

201   *Avena barbata* (19). To determine if differences in metabolic signals contribute to

202   bacterial community assemblage during drought in field grown sorghum, we performed

203   an untargeted liquid chromatography-mass spectrometry based metabolomic profiling of

204   root, rhizosphere, and soil, using the same samples as bacterial profiling described

205   above. Using a metabolite atlas as reference (43), 112 and 122 polar metabolites were

206   predicted in positive and negative ion modes, respectively, which were then combined

207   to give a total of 168 unique metabolites (supplemental figure 1, supplemental tables 1

208   and 2). Within these metabolites, we observed different patterns of enrichment across

209   both compartments and treatments, with individual metabolites that were either drought-

210   enriched or drought-depleted (figure 2a). Principal component analysis (PCA) was

211   performed to understand the relationships between samples. PC1 accounted for 59.5%

212   of the total variation and PC2 accounted for 17.1% of the variation, distinguishing

213   samples by both compartment and watering regime (figure 2b). Next, we aimed to

214   determine metabolites that were significantly enriched *(Log$_2$ fold change >2, t-test*

215   *p<0.05)* in each compartment during drought. Twenty-eight, 35, and 16 metabolites

216   were significantly enriched during drought in roots, rhizosphere, and soil, respectively

217   (supplemental table 3), with enrichment that was either compartment specific or

218   observed in multiple compartments (figure 2c).

219

220   Differences in metabolites observed between compartment and watering treatment

221   suggest that these factors may be responsible for driving associations between plants

222   and their root-associated microbiome. We hypothesized that metabolites with large

223   changes in relative abundance, or fold change, between drought and watered

224   treatments may be important for the observed shifts in the microbiome. In droughted

225   roots, we observed increases in the relative abundance of many putative abiotic stress

226   response factors, including amino acids, osmoprotectants, antioxidants, hormones, and

227   organic acids (figure 2d, table 1). Surprisingly, the important drought markers ABA, 1-

228   aminocyclopropane-1-carboxylic acid (1-ACC, the precursor to ethylene), proline and

229   betaine separated into three distinct clusters of enrichment (figure 2d). In contrast, only

230   3 metabolites were significantly more abundant in watered roots, including xylitol and

231   the phenolics 2,3-dihydroxybenzoic acid and 4-methylcatechol, which are direct

232   catabolism products of salicylic acid and methylsalicylate, respectively (44, 45) (figure

233   2e, table 1). Collectively, the observed metabolite enrichment patterns are consistent

234   with sorghum roots responding metabolically to drought.

235
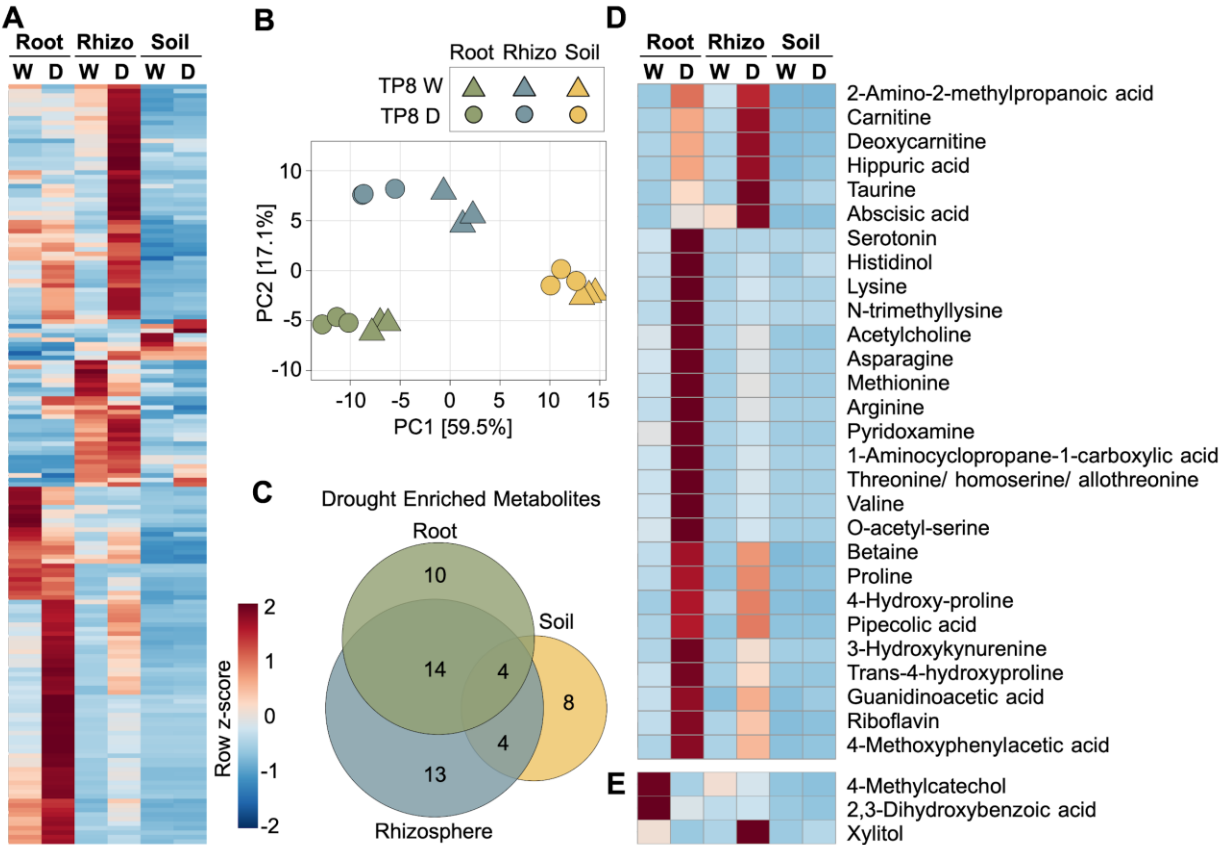
Figure 2. Metabolic profiles during drought differ by compartment. A *Heatmap of relative peak heights of all observed metabolites (n=168) across root, rhizosphere (rhizo), and soil compartments and watered (W) and drought (D) treatments. **B** Principal component analysis (PCA) plot of root, rhizosphere, and soil metabolites. **C** Proportional Venn diagram of drought enriched metabolites in root, rhizosphere, or soil (D/W Log$_2$ fold change >2, t-test p<0.05). **D-E** Heatmap of the subset of metabolites that were enriched or depleted in roots during drought, with the predicted identity of metabolites listed beside each row.*

12

Response to rewatering within 24 hours following a prolonged drought varies by

compartment

Having established that metabolite composition differs between watered and drought

sorghum roots, we next sought to understand whether rapid shifts in metabolite profiles

would be observed 24 hours after rewatering the droughted sorghum plots. We

hypothesized that rewatering would shift metabolite compositions, particularly in the

rhizosphere, that could contribute to the transitions observed in microbial community

composition. Consistent with this hypothesis, we observed distinct response patterns in

metabolites across all compartments 24 hours after rewatering the droughted plots.

Notably, roots were only weakly responsive to rewatering, with no metabolites strongly

enriched in rewatered roots (Log_2 fold change >2, t-test p<0.05) (figure 3a). However,

several metabolites were modestly enriched (Log_2 fold change >1, t-test p<0.05),

including cytosine, sphinganine, N-acetylglutamic acid, which promotes growth of root

hairs and swelling of root tips (46), and ferulic acid, which is capable of inhibiting root

growth and promotes root branching (47) (supplemental table 4). Collectively, these

shifts suggest roots have started to respond to changes in water availability, although

their overall metabolite profiles are largely unchanged at the time of sampling.

In contrast to roots, large shifts in metabolite abundances occurred in the rhizosphere

after rewatering, with rewatering tending to cause a depletion of rhizosphere

metabolites (figure 3a). Significantly depleted metabolites (n=17, Log_2 fold change < -2,

t-test p<0.05) included ten different organic acids, four sugar alcohols, sn-glycero-3-

phosphocholine, carnitine, and melatonin (figure 3b, table 2). In soil, only a single

13

270   metabolite, trehalose, was significantly depleted following rewatering (figure 3c, table 2).

271   Notably, the metabolite composition of rewatered rhizosphere became more similar to

272   watered rhizosphere, and was distinguishable from soil (figure 3d).

273

274

275

276   **Figure 3. Rewatering depletes rhizosphere metabolites following a prolonged**

277   **drought. A** *Heatmap of relative peak heights of all observed metabolites (n=168)*

278   *across three compartments (root, rhizosphere (rhizo), and soil), three treatments*

279   *(watered (W), drought (D), drought rewatered (DW), and two time points (time point 8*

14

280   *(TP8) and 24 hours later (24h)).* **B-C** *Heatmap of the subset of metabolites that were*

281   *depleted after rewatering (DW/D Log$_2$ fold change < -2, t-test p<0.05), with the*

282   *predicted identity of metabolites listed beside each row. Note, all significant depletions*

283   *were observed in the rhizosphere, except trehalose, which occurred in soil.* **D** *Principal*

284   *component analysis (PCA) plot of root, rhizosphere, and soil metabolites.*

285

286   **Pipecolic acid suppresses plant root growth**

287   Betaine represents one of the most robust and widely utilized biomarkers of plant

288   responses to drought (31, 48). We hypothesized that other metabolites with roles in

289   plant drought response would share a similar abundance pattern during drought. To

290   identify other putative drought metabolites, we ranked metabolites based on their

291   correlation coefficients (Pearson's r) with betaine, across all compartments, treatments,

292   and timepoints (figure 4a-c). The most strongly correlated metabolite, pipecolic acid

293   (Pip), is a lysine catabolite that has recently been identified as a critical component of

294   the systemic acquired resistance (SAR) pathway (41, 42). However, to our knowledge

295   no link between Pip and drought stress response has been demonstrated in plants,

296   although its synthesis is osmotically induced in rapeseed leaf discs (49) and in the

297   halophyte *Triglochin maritima* (50). Beyond Pip, the other nine of the top 10 correlated

298   metabolites have all been previously identified as drought-related metabolites. These

299   include 4-aminobutanoic acid (GABA) (51), allantoin (52, 53), carnitine (54, 55), and the

300   amino acids proline, tyrosine, asparagine, serine, glutamine, and trans-4-hydroxyproline

301   (56–60) (figure 4a).

302

15

303   To identify potential interactions between these drought-related metabolites and the

304   root-associated bacterial community, we clustered bacterial ASVs (grouped at the class

305   level) and metabolites based on abundances across all compartments, treatments, and

306   timepoints. Strikingly, while a majority of metabolites and microbes separated into

307   distinct clusters, three microbial taxa, including the Actinobacteria, nested within the

308   metabolite-dominant cluster, just adjacent to the metabolite cluster containing the top

309   ten betaine-correlated metabolites (supplemental figure 2). When clustering was

310   performed based on the abundances in the root, where host control of the microbiome

311   is strongest, we observed that the Actinobacteria formed an even closer linkage with

312   betaine-correlated metabolites, and was tightly clustered with five metabolites including

313   trans-4-hydroxyproline, proline, Pip, valine, and guanidinoacetic acid (figure 4e-f,

314   supplemental figure 3). As previous reports have demonstrated that drought-induced

315   microbial lineages including Actinobacteria in roots are capable of inducing SAR (61)

316   and systemic root-to-root signaling (62), we hypothesized that the increased abundance

317   of Actinobacteria in sorghum roots may contribute to the accumulation of Pip during

318   drought, and potentially the activation of systemic signaling. However, azelaic acid,

319   which functions downstream of Pip in the SAR pathway (63), was not enriched by

320   drought in our data, suggesting that SAR was not being activated (figure 4d).

321   Collectively, these results suggest that Pip may play an as-yet undiscovered role in

322   sorghum drought response.

323

324

325
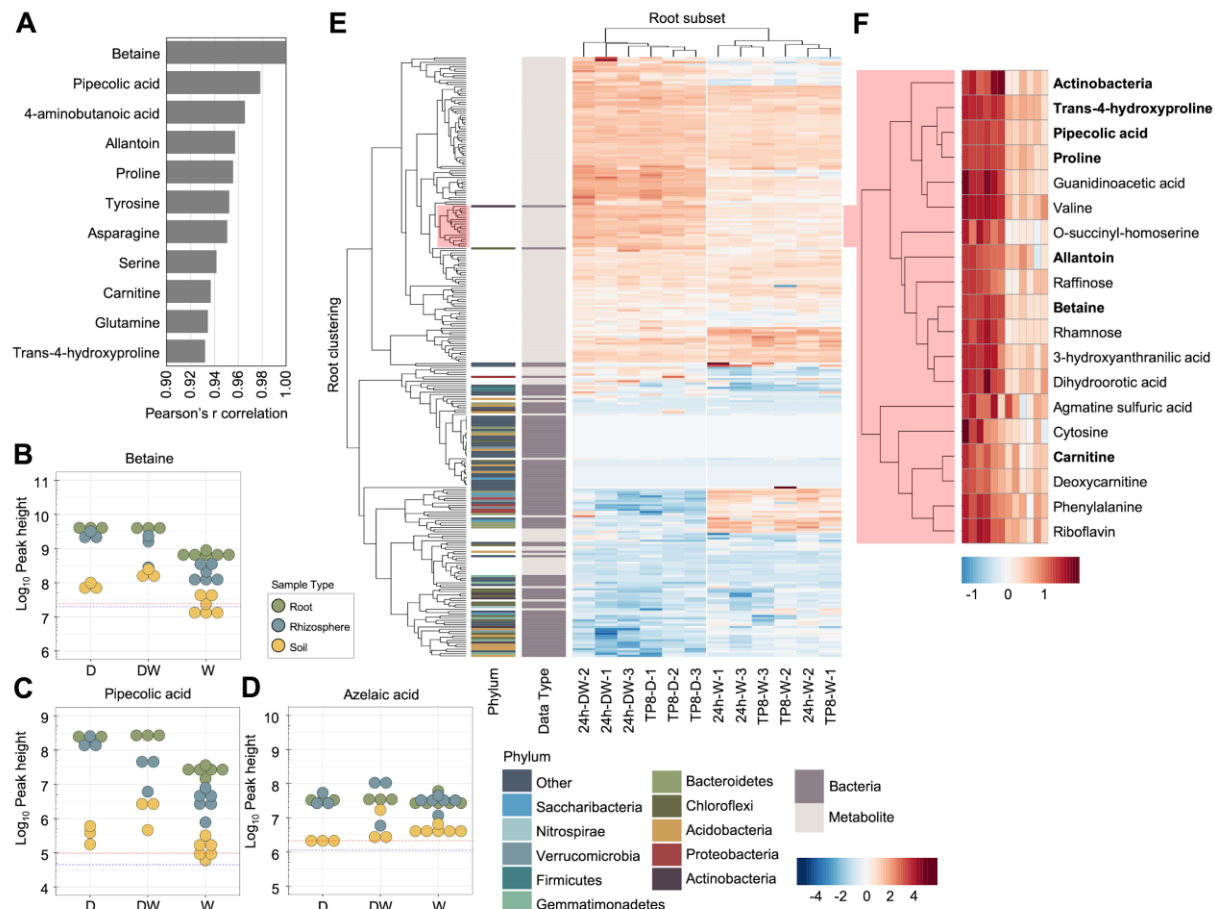
Figure 4. Pipecolic acid abundance pattern mirrors drought markers. *A The top 10 metabolites correlated with the drought marker betaine across all sample types, treatments, and time points. B-D Log$_{10}$ peak heights of individual metabolites. Each point represents an individual sample of root (green), rhizosphere (blue), or soil (yellow). Dashed lines represent the limit of detection for individual metabolites, based on the average log$_{10}$ peak heights of the sample blanks for root (red) or rhizosphere and soil (blue). E Heatmap of relative abundance of all metabolites and bacteria ASVs (grouped at the class level), clustered within the root, across treatments (watered (W), drought (D), drought rewatered (DW), and time points (time point 8 (TP8) and 24 hours later*

17

335 *(24h)). **F** Zoom-in of Actinobacteria and closely clustering root metabolites, as*

336 *highlighted in pink in figure 4e. Actinobacteria and the metabolites that are closely*

337 *correlated with betaine (as in figure 4a) are in bold.*

338

339 One classic and easily observable phenotypic shift that occurs in roots during drought is

340 a suppression of root growth (64, 65). We hypothesized that if Pip plays an integral role

341 in the drought response pathway, application of Pip should lead to reduced root growth.

342 To evaluate this possibility, we germinated sorghum in petri dishes containing water

343 plus 0, 0.1, or 1 mM Pip. Seven days after germination, 1 mM Pip treated sorghum

344 displayed significantly reduced root growth (figure 5a-b). Exogenous Pip application is

345 also capable of reducing root growth in *Arabidopsis* (66). We confirmed this result by

346 growing *Arabidopsis* Col-0 on petri dishes containing either 0, 0.001, 0.01, 0.1, 1 mM

347 Pip. Average root growth was reduced in all Pip treatments in a dosage dependent

348 manner, with significant decreases in root growth observed with 0.1 and 1 mM Pip

349 concentrations (figure 5c-d).

350
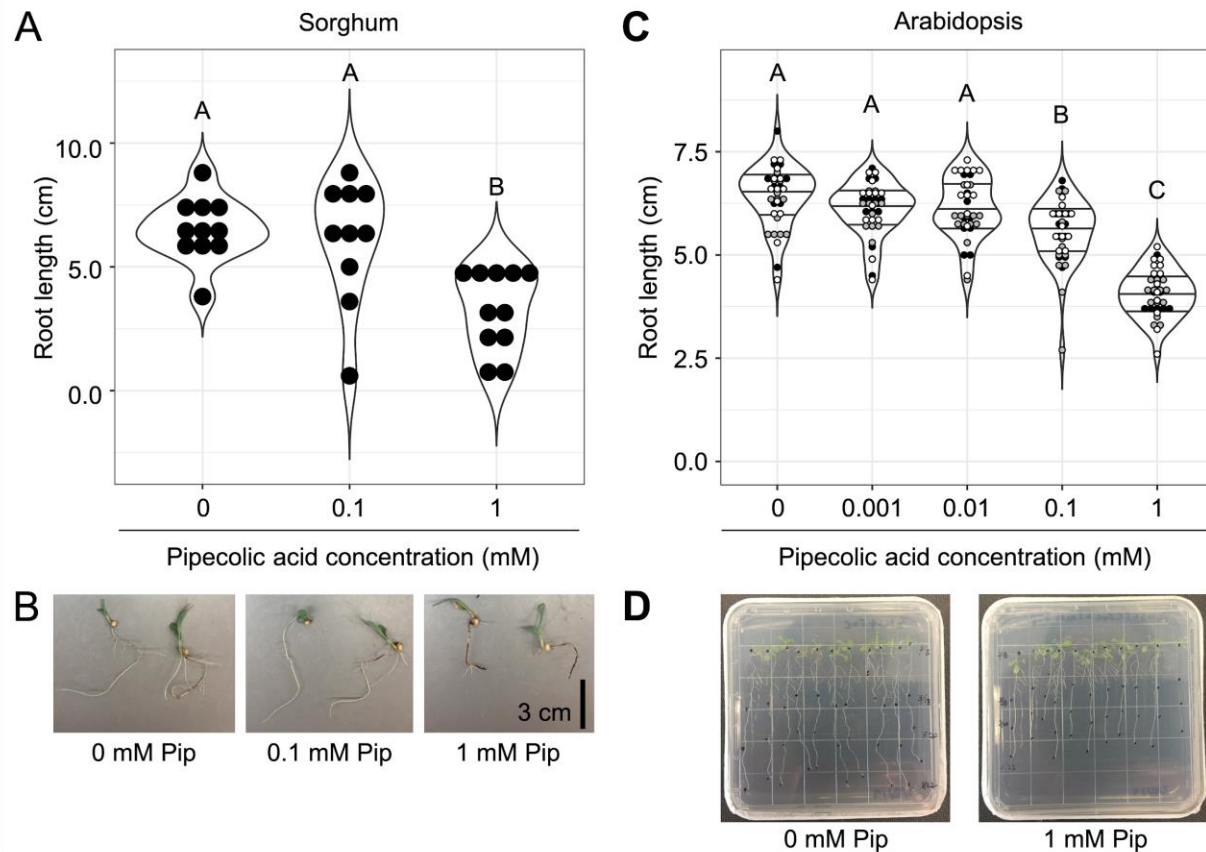
Figure 5. Pipecolic acid reduces root growth. A *Root lengths of sterilized sorghum seedlings after 7 days of growth in water containing 0, 0.1, or 1 mM pipecolic acid (Pip). Different letters indicate a significant difference in root length (ANOVA, Tukey-HSD, p<0.05). This experiment was performed twice with similar results.* **B** *Two representative seedlings from each treatment were photographed at the time of measurement.* **C** *Root lengths of sterilized Arabidopsis seedlings after 10 days of growth in ½ MS+ 1% sucrose agar media containing 0, 0.001, 0.01, 0.1, or 1 mM Pip. Different letters indicate a significant difference in root length (ANOVA, Tukey-HSD, p<0.05). Different colors represent plants from independent experiments (n=3).* **D** *One*

362 *representative plate from 0 and 1 mM pipecolic acid treatments were photographed at*

363 *the time of measurement.*

364

365 Having confirmed that exogenous Pip is sufficient to reduce root growth, we next aimed

366 to understand the molecular mechanism responsible for this behavior. As Pip plays a

367 key role in systemic signalling during SAR (67), we hypothesized that Pip-mediated root

368 growth reduction may depend on components of this signalling pathway. To test this

369 hypothesis, we utilized publicly available genetic resources in *Arabidopsis*, including

370 *fmo-1*, *npr1-1*, *rbohd/rbohf*, *azi1-2* mutants, which represent critical aspects of the SAR

371 signalling pathway (figure 6). We measured the root growth of each of these validated

372 *Arabidopsis* SAR mutants on media containing 1 mM Pip. Notably, mutants in FLAVIN-

373 CONTAINING MONOOXYGENASE 1 (FMO-1), responsible for conversion of Pip to N-

374 hydroxy-Pip (68)(figure 6), displayed reduced root growth similar to the wild-type plant

375 Col-0 in response to Pip (figure 6), indicating that this conversion is not required to elicit

376 reduced root growth. Likewise, mutants in NON EXPRESSER OF PATHOGENESIS

377 RELATED GENES 1 (NPR1) (69), a SA receptor required for SA-dependent SAR, and

378 mutants in NADPH/RESPIRATORY BURST OXIDASE PROTEINS D and F (RBOH

379 D/F) and the lipid transfer protein AZELAIC ACID INDUCED 1 (AZI1) (70, 71), required

380 for SA-independent SAR, also responded similar to Col-0 (figure 6).Collectively, these

381 data indicate that root growth response to Pip is likely not mediated by the SAR

382 pathway.

383
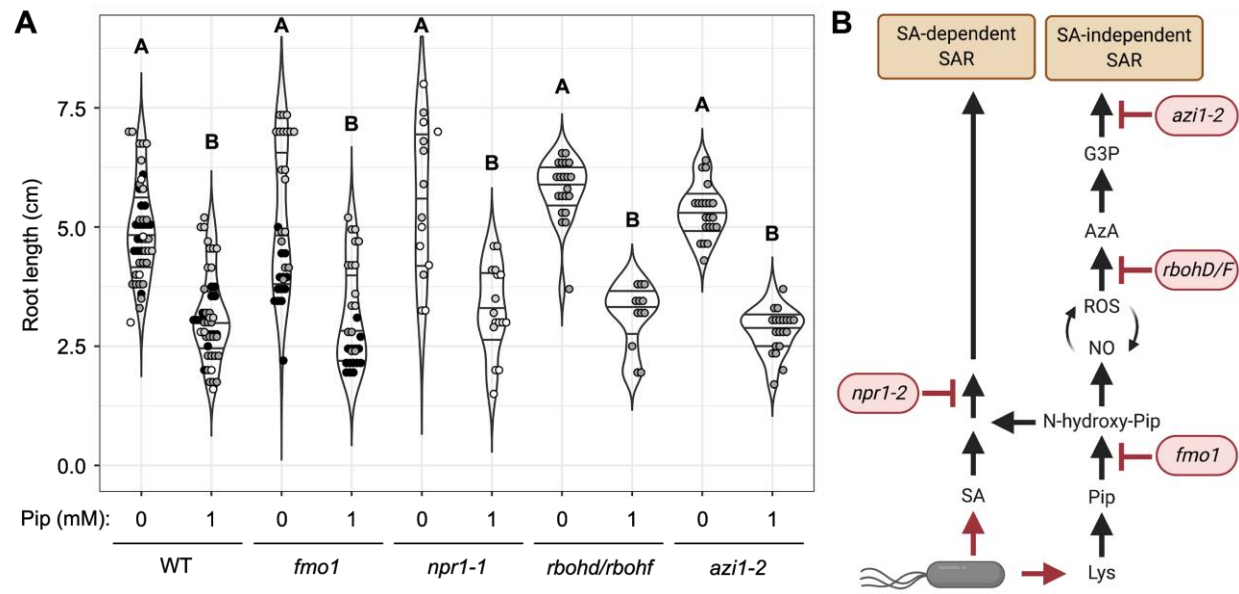
Figure 6. Pipecolic acid root growth reduction is SAR-independent. A *Root length of Arabidopsis Col-0 (WT) and Arabidopsis mutants grown on 1/2MS + 1% sucrose plates containing 0 or 1 mM Pip. Significance between treatments was evaluated by ANOVA with Tukey's HSD posthoc test (p<0.05). Different colors represent plants from independent experiments.* **B** *Simplified SAR pathway. Highlighted in red are the Arabidopsis mutants used to evaluate a potential interaction between SAR and Pip-mediated root growth suppression.*

DISCUSSION

Metabolite and microbial community compositions shift during drought and rewatering

The assemblage of the microbiomes differ between root, rhizosphere, and soil during drought, though the underlying cause of these differences is not well understood. Plant metabolites and exudates have been hypothesized to drive these changes (30), and

21

400   plants are known to increase total organic carbon and root exudation (per gram of root

401   biomass) in response to drought (72, 73). The enrichment of specific metabolites that

402   can act as osmoprotectants, such as betaine, sugars, and amino acids, is frequently

403   reported when plants are subjected to drought, and these are commonly used as

404   drought-specific markers. Yet, comprehensive studies of the global metabolite profiles

405   across root, rhizosphere, and soil have been hindered by the complexity of soil

406   metabolite profiles. However, recent advances in metabolomics have allowed for

407   characterization of metabolite profiles within and across complex substrates (74). As a

408   result, we collected both microbiome and metabolite profiles across three different

409   compartments (sorghum root, rhizosphere, and soil) and three treatments (watered,

410   drought, and drought recovery). We observed a general trend that many metabolites

411   were more abundant during drought. This observation is in line with previous evidence

412   that exudation by plants increases during drought (72). Interestingly, we observed both

413   shifts in metabolite abundances during drought that were compartment specific and

414   shifts that occurred across multiple compartments. Likewise, we observed enrichment of

415   specific drought responsive metabolites that correlated with increases in both

416   monoderm dominance during drought and compartment specific shifts upon rewatering.

417   Our findings that changes in host metabolism during drought are correlated with shifts in

418   certain bacterial taxa expand upon a recent finding that substrate utilization also drives

419   microbial community assembly in the rhizosphere across developmental age (19).

420

421   A previous study of sorghum root and rhizosphere showed that bacterial community

422   abundance reverts from monoderm dominance during drought to diderm dominance

423   within a week following rewatering (13). To understand the early dynamics of this

424   reversion, we evaluated sorghum root, rhizosphere, and soil at the peak of a

425   preflowering drought and again 24 hours after rewatering. We observed distinct

426   response patterns in metabolites of root, rhizosphere, and soil 24 hours after

427   rewatering, which could impact the establishment of microbiomes following rewatering.

428   Notably, the rhizosphere was the most responsive in both metabolites and microbiome

429   profiles within 24 hours after rewatering. We propose that the more rapid shifts

430   observed in rhizosphere are largely driven by flow of water, which may simultaneously

431   dilute rhizosphere metabolites into the surrounding soil, and promote the mobility of soil

432   microbes to enter the rhizosphere. Supporting this hypothesis, the beta diversity of

433   rewatered rhizosphere microbiome early after rewatering more closely resembled the

434   soil microbiome, rather than watered rhizosphere samples, suggesting that the soil

435   microbiome is a source of inoculum for bacterial establishment in the rhizosphere

436   following rewatering. In contrast, rhizosphere metabolites were characterized by

437   depletion after rewatering, with similarity to watered rhizosphere, which may facilitate

438   the eventual reversion to a watered rhizosphere microbiome, as demonstrated

439   previously (13). Comparable studies on the long-term effects of drought and subsequent

440   rewatering on metabolite profiles in grasses are lacking, however previous studies of

441   trees have reported mixed long-term effects. One study found that increases in

442   exudation can be reversed following recovery from drought, to be indistinguishable from

443   controls (73), while another found that extreme drought led to irreversible changes in

444   exudation (59). Therefore, future studies will benefit from careful selection of multiple

23

445   time points following drought to understand the long-term effects of drought in roots and

446   rhizosphere following rewatering.

447

Pipecolic acid-mediated root growth suppression is not mediated by the systemic acquired resistance pathway

450   In this study, we observed an enrichment of many putative abiotic stress response

451   factors during drought. Of particular note, Pip was significantly enriched during drought,

452   and its abundance correlated strongly with other highly enriched drought markers

453   including Actinobacteria and the metabolites betaine, proline, and GABA. While Pip

454   induction in response to osmotic stress has been noted in a few previous studies (49,

455   50), by far Pip's most notable role is in systemic signalling of stress in response to

456   pathogens. It has recently been shown that the conversion of Pip to N-hydroxy-Pip is

457   required for SAR to be activated, and this activity functions both alongside and

458   independent of SA (67, 75). Notably, previous research has demonstrated that "biotic

459   stress" factors, including SA, can benefit plants responding to abiotic stress. For

460   example, plant drought tolerance can be promoted by increasing endogenous SA in

461   *Arabidopsis* (76), and exogenous SA also promoted drought tolerance via an NPR1-

462   dependent mechanism in *Brassica napus* (77). However, recent studies suggest that SA

463   signaling is inactivated by drought, in part because ABA promotes NPR1 degradation

464   (33, 78). Additionally, a strong suppression of defense-related gene expression occurs

465   in field grown sorghum during preflowering drought (34). Likewise, we did not see an

466   enrichment of azelaic acid, which functions downstream of Pip during SAR, during

467   drought in our data. These findings suggest that the Pip induction observed during

468   drought is likely acting for some other purpose, perhaps as an independent signalling

469   mechanism related to abiotic stress.

470

471   Here, we demonstrate that Pip application is able to provoke one of the classic drought

472   responses in roots, namely root growth suppression (64, 65), which suggests it could be

473   involved in the drought response pathway. As exogenous Pip was capable of

474   suppressing root growth in both sorghum and *Arabidopsis*, this suggests that a common

475   mechanism is conserved across plants. We hypothesized that Pip-mediated root growth

476   suppression might share components with the SAR pathway, which functions across

477   diverse plant clades (79). However, using previously validated *Arabidopsis* SAR

478   pathway mutants, we demonstrate that this Pip activity in the root functions

479   independently from the established SAR pathway, which has primarily been evaluated

480   in leaves. These data suggest that although Pip has been primarily characterized as a

481   component of SAR in plants, it may also act as a more general stress response factor to

482   environmental shifts including drought using an alternative mechanism. Furthermore,

483   azelaic acid, another component of SAR that functions downstream of Pip, is not

484   enriched in sorghum roots under drought, which suggests that this pathway, if it exists,

485   acts differently than the one currently known example.

486

487   Interestingly, Pip, which was significantly enriched in both roots and rhizosphere, has

488   also been shown to have a direct role on microbes, where it is predicted to function in

489   osmoprotection. For example, Pip has been widely demonstrated to improve the growth

490   of a diverse bacteria challenged by NaCl-induced osmotic stress, including the

491   Actinobacteria lineage *Brevibacterium ammonkgenes* (80), and Proteobacteria lineages

492   *Escherichia coli* (81), *Sinorhizobium meliloti* (82), and *Silicibacter pomeroyi* (83).

493   Supporting its role as an osmoprotectant, exogenous application of another

494   osmoprotectant, betaine, suppressed the salt-induced accumulation of Pip (80). These

495   studies support a possible role of rhizosphere Pip acting as an osmolyte to protect

496   bacteria during drought. However, as Pip appears to be functional across a broad range

497   of bacterial lineages, we do not believe Pip is likely to be responsible for the shifts in

498   monoderm and diderm dominance observed during drought and subsequent rewatering.

499   Collectively, our results highlight the need for future studies that delve further into the

500   potential contribution(s) of Pip to plant drought responses.

501

502   **METHODS**

503   **Field experimental design and sample collection**

504   Sorghum cultivar RTx430 plants were grown in the summer of 2017, in a field located at

505   the UC-ANR KARE Center located in Parlier, California (36.6008 N 119.5109 W), as

506   described previously (13, 84). Sorghum seeds were sown into pre-watered fields.

507   Starting in the third week, control treatment plants were watered 1h three times per

508   week by drip irrigation (1.89 L h^{-1} flow rate), and no water was provided to drought

509   treatment plants. After eight weeks, which coincided with the onset of flowering, roots

510   and rhizosphere samples were harvested prior to watering (TP8). Water was then

511   restored to the drought plots (rewatered), and root and rhizosphere samples were

512   harvested after 24 h (TP8+24h). All field samples were collected between 11am and

513   12pm using a modified version of the protocol described in detail in (85). Soil samples

26

514 were collected using a 15 cm soil core sampler, at a distance of approximately 20 cm

515 from the base of the plant. To collect rhizosphere compatible with both microbiome and

516 metabolomic analyses, excavated plants were briefly shaken to dislodge excess soil,

517 and an ethanol-sterilized nylon bristled toothbrush was used to remove closely adhering

518 soil from the root, which we collected as the rhizosphere fraction, prior to vortexing the

519 roots two times for 1 min in epiphyte removal buffer (ice cold 0.75% KH_2PO_4, 0.95%

520 K_2HPO_4, 1% Triton X-100 in ddH_2O; filter sterilized at 0.2 µM). Any remaining soil

521 adhering to the root was separated with epiphyte removal buffer and discarded. The

522 roots were again rinsed with clean epiphyte removal buffer and patted dry. All samples

523 were immediately flash frozen in LN_2 in the field and stored at -80 °C until sample

524 processing.

525

526 DNA extraction, amplification, and amplicon sequencing

527 DNA extraction was performed using the protocol for collection of root endosphere,

528 rhizosphere, and soil samples using Qiagen DNeasy Powersoil DNA extraction Kit with

529 0.15 g (root) and 0.25 g (rhizosphere and soil) as starting material in the provided

530 Powersoil collection vials, as described in detail in (85). The V3-V4 region of the 16S

531 rRNA gene was PCR amplified from 25 ng of genomic DNA using dual-indexed 16S

532 rRNA Illumina iTags 341F (5'-CCTACGGGNBGCASCAG-3') and 785R (5'-

533 GACTACNVGGGTATCTAATCC-3'). Barcoded 16S rRNA amplicons were quantified

534 using Qubit dsDNA HS assay kit on a Qubit 3.0 fluorometer (Invitrogen, Carlsbad, CA,

535 USA), pooled in equimolar concentrations, purified using Agencourt AMPure XP

536 magnetic beads (Beckman Coulter, Indianapolis, IN, USA), quantified using Qubit

537   dsDNA HS assay kit on a Qubit 3.0 fluorometer (Invitrogen, Carlsbad, CA, USA), and

538   diluted to 10 nM in 30 μL total volume before submitting to the QB3 Vincent J. Coates

539   Genomics Sequencing Laboratory facility at the University of California, Berkeley for

540   sequencing using Illumina Miseq 300 bp pair-end with v3 chemistry.

541

542   **Amplicon sequence processing and analysis**

543   16S amplicon sequencing reads were demultiplexed in QIIME2 (86) and then passed to

544   DADA2 (87) to generate Amplicon Sequence Variants (ASVs), with taxonomies

545   assigned using the August 2013 version of GreenGenes 16S rRNA gene database as

546   described previously (16). All subsequent 16S statistical analyses were performed in R-

547   v3.6.1 (88). To account for differences in sequencing read depth across samples,

548   samples were normalized by dividing the reads per ASV in a sample by the sum of

549   usable reads in that sample, resulting in a table of relative abundance frequencies,

550   which were used for analyses, with the exception of alpha-diversity calculations, for

551   which all samples were normalized to an even read depth of 29,918 ASVs per sample.

552   Alpha diversity was determined with the estimate_richness function in the R package

553   phyloseq-v1.30.0 (89), and significance was tested by ANOVA using the aov function in

554   the R stats package. Beta diversity (PCoA) was performed using the ordinate function in

555   the R package phyloseq-v1.30.0 (89). Sample type separation was determined by

556   pairwise PERMANOVA with 1,000 permutations using the adonis and

557   calc_pairwise_permanovas functions in the R packages vegan-v2.5.6 (90) and

558   mctoolsr-v0.1.1.2. Tukey-HSD tests used the HSD.test function in the R package

28

559   Agricolae-v1.3.1. The combined metabolite and bacterial ASV heatmaps were

560   generated using the R package pheatmap-v1.0.12.

561

562   **Metabolite extraction and LC-MS**

563   Root water content was estimated by lyophilizing root tissue and calculating the

564   difference between wet and dry weights. Root samples for submission were then

565   normalized such that the lightest sample was 0.2 g (wet weight) and each other sample

566   was at least 0.2 g. Rhizosphere and soil water contents were estimated to obtain similar

567   amounts of material. The overall difference in percent water content between samples

568   was minimal (2.5-6.5%). For extraction of polar metabolites from root tissue (0.2-0.3 g

569   wet weight), samples were first lyophilized dry, then 500 µL of methanol was added,

570   followed by a brief vortex and sonication in a water bath for 10 min. Samples were

571   centrifuged 5 min at 5,000 rpm, then supernatant transferred to 2 mL tubes, dried in a

572   SpeedVac (SPD111V, Thermo Scientific, Waltham, MA), and extracts stored at -80 °C.

573   For soil and rhizosphere samples (1.25 g wet weight), polar metabolites were extracted

574   similarly but samples were not lyophilized prior to extraction, 2 mL LC-MS grade water

575   was added followed by vortex and water bath sonication for 30 min, centrifugation for 7

576   min at 7,000 rpm, then supernatant transferred to a 5 mL tube, frozen and lyophilized

577   dry, and extracts stored at -80 °C.

578

579   In preparation for LC-MS, soil and rhizosphere extracts were resuspended with 300 µL

580   methanol containing internal standards (~15 µM average of 5-50 µM of 13C,15N Cell

581   Free Amino Acid Mixture; 4-(3,3-dimethyl-ureido)benzoic acid; 3,6-dihydroxy-4-

29

582   methylbenzoic acid; d5-benzoic acid; 9-anthracene carboxylic acid; 13C-trehalose; 13C-

583   mannitol), vortexed and sonicated 10 min, centrifuged 5 min at 5,000 rpm, supernatant

584   centrifuge-filtered 2.5 min at 2 500 rpm (0.22 μm hydrophilic PVDF), then 150 μL

585   transferred to LC-MS glass autosampler vials. Root extracts were resuspended

586   similarly, but with resuspension volume varied to normalize by root dry weight.

587

588   Chromatography was performed using an Agilent 1,290 LC stack, with MS and MS/MS

589   data collected using a Thermo QExactive Orbitrap MS (Thermo Scientific, Waltham,

590   MA). Full MS spectra were collected from m/z 70-1,050 at 70,000 resolution in both

591   positive and negative ion modes, with MS/MS fragmentation data acquired using

592   stepped 10, 20, and 40 eV collision energies at 17,500 resolution. Chromatography was

593   performed using a HILIC column (Agilent InfinityLab Poroshell 120 HILIC-Z, 2.1 x 150

594   mm, 2.7 μm, #673775-924) at a flow rate of 0.45 mL/min with a 2 μL injection volume.

595   To detect metabolites, samples were run on the HILIC column at 40 ºC equilibrated with

596   100% buffer B (95:5 ACN:H2O with 5 mM ammonium acetate) for 1 min, diluting buffer

597   B down to 89% with buffer A (100% H2O with 5 mM ammonium acetate and 5 μM

598   methylenediphosphonic acid) over 10 min, down to 70% B over 4.75 min, then down to

599   20% B over 0.5 min, followed by isocratic elution in 80% buffer A for 2.25 min. Samples

600   consisted of 3 biological replicates each and 3 extraction controls, with sample injection

601   order randomized and an injection blank (2 μL MeOH) run between each sample.

602

603   **Metabolite identification and analysis**

604   Metabolite identification was based on exact mass and comparing retention time (RT)

605   and MS/MS fragmentation spectra to that of standards run using the same

606   chromatography and MS/MS method. Custom Python code (91) was used to analyze

607   LC-MS data. For each feature detected (unique m/z coupled with RT), a score (0 to 3)

608   was assigned representing the level of confidence in the metabolite identification.

609   Positive identification of a metabolite had detected m/z ≤ 5 ppm or 0.001 Da from

610   theoretical as well as RT ≤ 0.5 min compared to a pure standard run using the same

611   LC-MS method. The highest level of positive identification (score of 3) for a metabolite

612   also had matching MS/MS fragmentation spectra compared to either an outside

613   database (METLIN) (92) or internal database generated from standards run and

614   collected on a QExactive Orbitrap MS. Identifications were invalidated if MS/MS from

615   the sample mismatched that of the standard. MS/MS mirror plots for metabolites are

616   presented in supplemental figure 1.

617

618   A total of 112 and 122 polar metabolites were predicted in positive and negative ion

619   modes respectively (supplemental table 1). If a metabolite was observed in both ion

620   modes, the mode with higher peak height was selected for the merged metabolite

621   profile (n=168) used for all analyses. Values below the limit of detection were imputed

622   with the lowest observed values in the dataset rounded down (2,400 or 1,900 for

623   positive or negative ion modes respectively) (supplemental table 2). Principal

624   components analysis of metabolite profiles was performed using the prcomp function in

625   the R stats package. Venn diagram construction utilized Venny-v2.1.0 (93). All other

626   metabolite analyses were performed using MetaboAnalyst-v4.0 (94, 95). Heatmaps

627   were generated using Euclidean distance and Ward clustering algorithms. We

628   evaluated enriched or depleted metabolites with the cutoffs of $\log_2$ fold change greater

629   than 2 or less than -2, and a p-value of less than 0.05.

630

631   **Plant root growth assays**

632   Sterilized seeds of the sorghum cultivar RTx430 were germinated on petri dishes with

633   autoclaved Milli-Q water or autoclaved Milli-Q water containing the defined

634   concentration of Pip overnight in the dark at 28 °C, before being transferred to a growth

635   chamber (28/22 °C, 16 h day, ppf ~250 µmol m^{-2}s^{-1}). The *Arabidopsis* ecotype Columbia

636   (Col-0) was used in this study. Mutant lines *fmo-1* (SALK_026163) (96), *npr1-1*

637   (CS3726) (97), *rbohd/rbohf* (CS68522) (98), and *azi1-2* (SALK_085727) (70) were

638   obtained from the Arabidopsis Biological Resource Center (99). Sterilized seeds were

639   grown on MS plates containing 1/2× Murashige and Skoog salt mix, 1% sucrose (pH

640   5.8), 0.8% agar, and the defined concentration of Pip. Plants were first stratified for 3

641   days at 4°C before being transferred to a growth chamber (21 °C, 16 h day, ppf ~120

642   µmol m^{-2}s^{-1}). Root lengths were measured using ImageJ-v1.52a software (100). ANOVA

643   was performed using the aov function in the R stats package and Tukey-HSD tests

644   used the HSD.test function in the R package Agricolae-v1.3.1. SAR pathway image in

645   figure 6b was created with BioRender.com.

646

647   **Data availability**

648   All datasets and scripts for analysis are available through github

649   (https://github.com/colemanderr-lab/Caddell-2020) and all short read data can be

32

650   accessed through NCBI BioProject PRJNA655744. Raw metabolomics data will be

651   made available through the Joint Genome Institute Genome Portal.

652

653   **Acknowledgements**

654   We thank Dr. Edi Wipf for their helpful discussions and critical reading of the

655   manuscript.

656

657   **Author contributions**

658   D.C. conceived and designed the experiments, performed the experiments, analyzed

659   the data, and prepared figures and/or tables; K.L.,B.B., and T.N. performed the LC-MS,

660   metabolite identification, and analyzed the data; E.P. analyzed the data and prepared

661   figures and/or tables; J.S., J.H., and J.D. performed the field experiment; D.C-D.

662   conceived and designed the experiments and analyzed the data; All authors authored or

663   reviewed drafts of the paper and approved the final draft.

664

665   **References cited**

666   1.   Zolla G, Badri DV, Bakker MG, Manter DK, Vivanco JM. 2013. Soil microbiomes

667   vary in their ability to confer drought tolerance to Arabidopsis. Appl Soil Ecol 68:1–

668   9.

669   2.   Bulgarelli D, Rott M, Schlaeppi K, Ver Loren van Themaat E, Ahmadinejad N,

670   Assenza F, Rauf P, Huettel B, Reinhardt R, Schmelzer E, Peplies J, Gloeckner FO,

671   Amann R, Eickhorst T, Schulze-Lefert P. 2012. Revealing structure and assembly

672   cues for Arabidopsis root-inhabiting bacterial microbiota. Nature 488:91–95.

673 3. Lundberg DS, Lebeis SL, Paredes SH, Yourstone S, Gehring J, Malfatti S,

674   Tremblay J, Engelbrektson A, Kunin V, Del Rio TG, Edgar RC, Eickhorst T, Ley RE,

675   Hugenholtz P, Tringe SG, Dangl JL. 2012. Defining the core Arabidopsis thaliana

676   root microbiome. Nature 488:86–90.

677 4. Peiffer JA, Spor A, Koren O, Jin Z, Tringe SG, Dangl JL, Buckler ES, Ley RE. 2013.

678   Diversity and heritability of the maize rhizosphere microbiome under field

679   conditions. Proc Natl Acad Sci U S A 110:6548–6553.

680 5. Ofek-Lalzar M, Sela N, Goldman-Voronov M, Green SJ, Hadar Y, Minz D. 2014.

681   Niche and host-associated functional signatures of the root surface microbiome. Nat

682   Commun 5:4950.

683 6. Naylor D, DeGraaf S, Purdom E, Coleman-Derr D. 2017. Drought and host

684   selection influence bacterial community dynamics in the grass root microbiome.

685   ISME J.

686 7. Fitzpatrick CR, Copeland J, Wang PW, Guttman DS, Kotanen PM, Johnson MTJ.

687   2018. Assembly and ecological function of the root microbiome across angiosperm

688   plant species. Proc Natl Acad Sci U S A 115:E1157–E1165.

689 8. Edwards J, Johnson C, Santos-Medellín C, Lurie E, Podishetty NK, Bhatnagar S,

690   Eisen JA, Sundaresan V. 2015. Structure, variation, and assembly of the root-

691   associated microbiomes of rice. Proc Natl Acad Sci U S A 112:E911–20.

692 9. Haney CH, Samuel BS, Bush J, Ausubel FM. 2015. Associations with rhizosphere

693   bacteria can confer an adaptive advantage to plants. Nat Plants 1.

694   10. Walitang DI, Kim C-G, Kim K, Kang Y, Kim YK, Sa T. 2018. The influence of host

695   genotype and salt stress on the seed endophytic community of salt-sensitive and

696   salt-tolerant rice cultivars. BMC Plant Biol 18:51.

697   11. Chaparro JM, Badri DV, Vivanco JM. 2014. Rhizosphere microbiome assemblage is

698   affected by plant development. ISME J 8:790–803.

699   12. Edwards JA, Santos-Medellín CM, Liechty ZS, Nguyen B, Lurie E, Eason S, Phillips

700   G, Sundaresan V. 2018. Compositional shifts in root-associated bacterial and

701   archaeal microbiota track the plant life cycle in field-grown rice. PLoS Biol

702   16:e2003862.

703   13. Xu L, Naylor D, Dong Z, Simmons T, Pierroz G, Hixson KK, Kim Y-M, Zink EM,

704   Engbrecht KM, Wang Y, Gao C, DeGraaf S, Madera MA, Sievert JA, Hollingsworth

705   J, Birdseye D, Scheller HV, Hutmacher R, Dahlberg J, Jansson C, Taylor JW,

706   Lemaux PG, Coleman-Derr D. 2018. Drought delays development of the sorghum

707   root microbiome and enriches for monoderm bacteria. Proc Natl Acad Sci U S A

708   201717308.

709   14. Santos-Medellín C, Edwards J, Liechty Z, Nguyen B, Sundaresan V. 2017. Drought

710   Stress Results in a Compartment-Specific Restructuring of the Rice Root-

711   Associated Microbiomes. MBio 8.

712   15. Koyama A, Steinweg JM, Haddix ML, Dukes JS, Wallenstein MD. 2018. Soil

713   bacterial community responses to altered precipitation and temperature regimes in

714   an old field grassland are mediated by plants. FEMS Microbiol Ecol 94.

715   16. Simmons T, Styer AB, Pierroz G, Gonçalves AP, Pasricha R, Hazra AB, Bubner P,

716   Coleman-Derr D. 2020. Drought Drives Spatial Variation in the Millet Root

717   Microbiome. Front Plant Sci 11:599.

718   17. Baraniya D, Nannipieri P, Kublik S, Vestergaard G, Schloter M, Schöler A. 2018.

719   The Impact of the Diurnal Cycle on the Microbial Transcriptome in the Rhizosphere

720   of Barley. Microb Ecol 75:830–833.

721   18. Chaparro JM, Badri DV, Bakker MG, Sugiyama A, Manter DK, Vivanco JM. 2013.

722   Root exudation of phytochemicals in Arabidopsis follows specific patterns that are

723   developmentally programmed and correlate with soil microbial functions. PLoS One

724   8:e55731.

725   19. Zhalnina K, Louie KB, Hao Z, Mansoori N, da Rocha UN, Shi S, Cho H, Karaoz U,

726   Loqué D, Bowen BP, Firestone MK, Northen TR, Brodie EL. 2018. Dynamic root

727   exudate chemistry and microbial substrate preferences drive patterns in

728   rhizosphere microbial community assembly. Nat Microbiol 3:470–480.

729   20. Wallace JG, Kremling KA, Kovar LL, Buckler ES. 2018. Quantitative Genetics of the

730   Maize Leaf Microbiome. Phytobiomes Journal 2:208–224.

731   21. Badri DV, Chaparro JM, Zhang R, Shen Q, Vivanco JM. 2013. Application of natural

732   blends of phytochemicals derived from the root exudates of Arabidopsis to the soil

733   reveal that phenolic-related compounds predominantly modulate the soil

734   microbiome. J Biol Chem 288:4502–4512.

735   22. Zhang N, Wang D, Liu Y, Li S, Shen Q, Zhang R. 2014. Effects of different plant

736   root exudates and their organic acid components on chemotaxis, biofilm formation

737   and colonization by beneficial rhizosphere-associated bacterial strains. Plant Soil

738   374:689–700.

739 23. Huang AC, Jiang T, Liu Y-X, Bai Y-C, Reed J, Qu B, Goossens A, Nützmann H-W,

740   Bai Y, Osbourn A. 2019. A specialized metabolic network selectively modulates

741   Arabidopsis root microbiota. Science 364.

742 24. Cai T, Cai W, Zhang J, Zheng H, Tsou AM, Xiao L, Zhong Z, Zhu J. 2009. Host

743   legume-exuded antimetabolites optimize the symbiotic rhizosphere. Mol Microbiol

744   73:507–517.

745 25. Bressan M, Roncato M-A, Bellvert F, Comte G, Haichar FZ, Achouak W, Berge O.

746   2009. Exogenous glucosinolate produced by Arabidopsis thaliana has an impact on

747   microbes in the rhizosphere and plant roots. ISME J 3:1243–1257.

748 26. Iven T, König S, Singh S, Braus-Stromeyer SA, Bischoff M, Tietze LF, Braus GH,

749   Lipka V, Feussner I, Dröge-Laser W. 2012. Transcriptional activation and

750   production of tryptophan-derived secondary metabolites in arabidopsis roots

751   contributes to the defense against the fungal vascular pathogen Verticillium

752   longisporum. Mol Plant 5:1389–1402.

753 27. Wang Y, Bouwmeester K, van de Mortel JE, Shan W, Govers F. 2013. A novel

754   Arabidopsis-oomycete pathosystem: differential interactions with Phytophthora

755   capsici reveal a role for camalexin, indole glucosinolates and salicylic acid in

756   defence. Plant Cell Environ 36:1192–1203.

757   28. Wang Z, Zhang J, Wu F, Zhou X. 2018. Changes in rhizosphere microbial

758   communities in potted cucumber seedlings treated with syringic acid. PLoS One

759   13:e0200007.

760   29. Hu L, Robert CAM, Cadot S, Zhang X, Ye M, Li B, Manzo D, Chervet N, Steinger T,

761   van der Heijden MGA, Schlaeppi K, Erb M. 2018. Root exudate metabolites drive

762   plant-soil feedbacks on growth and defense by shaping the rhizosphere microbiota.

763   Nat Commun 9:2738.

764   30. Xu L, Coleman-Derr D. 2019. Causes and consequences of a conserved bacterial

765   root microbiome response to drought stress. Curr Opin Microbiol 49:1–6.

766   31. Caddell DF, Deng S, Coleman-Derr D. 2019. Role of the Plant Root Microbiome in

767   Abiotic Stress Tolerance, p. 273–311. *In* Verma, SK, White, Jr, Francis, J (eds.),

768   Seed Endophytes: Biology and Biotechnology. Springer International Publishing,

769   Cham.

770   32. Bostock RM, Pye MF, Roubtsova TV. 2014. Predisposition in plant disease:

771   exploiting the nexus in abiotic and biotic stress perception and response. Annu Rev

772   Phytopathol 52:517–549.

773   33. Yasuda M, Ishikawa A, Jikumaru Y, Seki M, Umezawa T, Asami T, Maruyama-

774   Nakashita A, Kudo T, Shinozaki K, Yoshida S, Nakashita H. 2008. Antagonistic

775   interaction between systemic acquired resistance and the abscisic acid-mediated

776   abiotic stress response in Arabidopsis. Plant Cell 20:1678–1692.

777   34. Varoquaux N, Cole B, Gao C, Pierroz G, Baker CR, Patel D, Madera M, Jeffers T,

778   Hollingsworth J, Sievert J, Yoshinaga Y, Owiti JA, Singan VR, DeGraaf S, Xu L,

779   Blow MJ, Harrison MJ, Visel A, Jansson C, Niyogi KK, Hutmacher R, Coleman-Derr

780   D, O'Malley RC, Taylor JW, Dahlberg J, Vogel JP, Lemaux PG, Purdom E. 2019.

781   Transcriptomic analysis of field-droughted sorghum from seedling to maturity

782   reveals biotic and metabolic responses. Proc Natl Acad Sci U S A.

783 35. Sheflin AM, Chiniquy D, Yuan C, Goren E, Kumar I, Braud M, Brutnell T, Eveland

784   AL, Tringe S, Liu P, Kresovich S, Marsh EL, Schachtman DP, Prenni JE. 2019.

785   Metabolomics of sorghum roots during nitrogen stress reveals compromised

786   metabolic capacity for salicylic acid biosynthesis. Plant Direct 3:e00122.

787 36. Castrillo G, Teixeira PJPL, Paredes SH, Law TF, de Lorenzo L, Feltcher ME, Finkel

788   OM, Breakfield NW, Mieczkowski P, Jones CD, Paz-Ares J, Dangl JL. 2017. Root

789   microbiota drive direct integration of phosphate stress and immunity. Nature

790   543:513–518.

791 37. Hein JW, Wolfe GV, Blee KA. 2008. Comparison of rhizosphere bacterial

792   communities in Arabidopsis thaliana mutants for systemic acquired resistance.

793   Microb Ecol 55:333–343.

794 38. Carvalhais LC, Dennis PG, Badri DV, Kidd BN, Vivanco JM, Schenk PM. 2015.

795   Linking Jasmonic Acid Signaling, Root Exudates, and Rhizosphere Microbiomes.

796   Mol Plant Microbe Interact 28:1049–1058.

797 39. Liu H, Carvalhais LC, Schenk PM, Dennis PG. 2017. Effects of jasmonic acid

798   signalling on the wheat microbiome differ between body sites. Sci Rep 7:41766.

799   40. Lebeis SL, Paredes SH, Lundberg DS, Breakfield N, Gehring J, McDonald M,

800   Malfatti S, Glavina del Rio T, Jones CD, Tringe SG, Dangl JL. 2015. PLANT

801   MICROBIOME. Salicylic acid modulates colonization of the root microbiome by

802   specific bacterial taxa. Science 349:860–864.

803   41. Návarová H, Bernsdorff F, Döring A-C, Zeier J. 2012. Pipecolic acid, an

804   endogenous mediator of defense amplification and priming, is a critical regulator of

805   inducible plant immunity. Plant Cell 24:5123–5141.

806   42. Bernsdorff F, Döring A-C, Gruner K, Schuck S, Bräutigam A, Zeier J. 2016.

807   Pipecolic Acid Orchestrates Plant Systemic Acquired Resistance and Defense

808   Priming via Salicylic Acid-Dependent and -Independent Pathways. Plant Cell

809   28:102–129.

810   43. Bowen BP, Northen TR. 2010. Dealing with the unknown: metabolomics and

811   metabolite atlases. J Am Soc Mass Spectrom 21:1471–1476.

812   44. Cámara B, Bielecki P, Kaminski F, dos Santos VM, Plumeier I, Nikodem P, Pieper

813   DH. 2007. A gene cluster involved in degradation of substituted salicylates via ortho

814   cleavage in Pseudomonas sp. strain MT1 encodes enzymes specifically adapted for

815   transformation of 4-methylcatechol and 3-methylmuconate. J Bacteriol 189:1664–

816   1674.

817   45. Zhang K, Halitschke R, Yin C, Liu C-J, Gan S-S. 2013. Salicylic acid 3-hydroxylase

818   regulates Arabidopsis leaf longevity by mediating salicylic acid catabolism. Proc

819   Natl Acad Sci U S A 110:14807–14812.

820   46. Philip-Hollingsworth$ S, Hollingsworth RI, Dazzo ST FB. 1991. N-Acetylglutamic

821   Acid: An Extracellular nod Signal of Rhizobium trifolii ANUS43 That Induces Root

822   Hair Branching and Nodule-like Primordia in White Clover Roots. Plan Perspect

823   16854:16858.

824   47. Caspersen S, Sundin P, Munro M, Aðalsteinsson S, Hooker JE, Jensén P. 1999.

825   Interactive effects of lettuce (Lactuca sativa L.), irradiance, and ferulic acid in

826   axenic, hydroponic culture. Plant Soil 210:115–126.

827   48. Sakamoto A, Murata N. 2000. Genetic engineering of glycinebetaine synthesis in

828   plants: current status and implications for enhancement of stress tolerance. J Exp

829   Bot 51:81–88.

830   49. Moulin M, Deleu C, Larher F, Bouchereau A. 2006. The lysine-ketoglutarate

831   reductase-saccharopine dehydrogenase is involved in the osmo-induced synthesis

832   of pipecolic acid in rapeseed leaf tissues. Plant Physiol Biochem 44:474–482.

833   50. Goas G, Goas M, Larher F. 1976. Formation de l'acide pipécolique chez Triglochin

834   maritima. Can J Bot 54:1221–1227.

835   51. Bown AW, Shelp BJ. 2016. Plant GABA: Not Just a Metabolite. Trends Plant Sci

836   21:811–813.

837   52. Nourimand M, Todd CD. 2017. Allantoin contributes to the stress response in

838   cadmium-treated Arabidopsis roots. Plant Physiol Biochem 119:103–109.

839   53. Irani S, Todd CD. 2018. Exogenous allantoin increases Arabidopsis seedlings

840   tolerance to NaCl stress and regulates expression of oxidative stress response

41

841   genes. J Plant Physiol 221:43–50.

842 54. Khan N, Bano A, Babar MA. 2019. Metabolic and physiological changes induced by

843   plant growth regulators and plant growth promoting rhizobacteria and their impact

844   on drought tolerance in Cicer arietinum L. PLoS One 14:e0213040.

845 55. Oney-Birol S. 2019. Exogenous L-Carnitine Promotes Plant Growth and Cell

846   Division by Mitigating Genotoxic Damage of Salt Stress. Sci Rep 9:17229.

847 56. Ranieri A, Bernardi R, Lanese P, Soldatini GF. 1989. Changes in free amino acid

848   content and protein pattern of maize seedlings under water stress. Environ Exp Bot

849   29:351–357.

850 57. Rai VK. 2002. Role of amino acids in plant responses to stresses. Biol Plant.

851 58. Fang Y, Xiong L. 2015. General mechanisms of drought response and their

852   application in drought resistance improvement in plants. Cell Mol Life Sci 72:673–

853   689.

854 59. Gargallo-Garriga A, Preece C, Sardans J, Oravec M, Urban O, Peñuelas J. 2018.

855   Root exudate metabolomes change under drought and show limited capacity for

856   recovery. Sci Rep 8:12696.

857 60. Fàbregas N, Fernie AR. 2019. The metabolic response to drought. J Exp Bot

858   70:1077–1085.

859 61. Conn VM, Walker AR, Franco CMM. 2008. Endophytic actinobacteria induce

860   defense pathways in Arabidopsis thaliana. Mol Plant Microbe Interact 21:208–218.

861   62. Korenblum E, Dong Y, Szymanski J, Panda S, Jozwiak A, Massalha H, Meir S,

862   Rogachev I, Aharoni A. 2020. Rhizosphere microbiome mediates systemic root

863   metabolite exudation by root-to-root signaling. Proc Natl Acad Sci U S A 117:3874–

864   3883.

865   63. Wang C, Liu R, Lim G-H, de Lorenzo L, Yu K, Zhang K, Hunt AG, Kachroo A,

866   Kachroo P. 2018. Pipecolic acid confers systemic immunity by regulating free

867   radicals. Sci Adv 4:eaar4509.

868   64. Tsuji W, Inanaga S, Araki H, Morita S, An P, Sonobe K. 2005. Development and

869   Distribution of Root System in Two GrainSorghum Cultivars Originated from Sudan

870   under Drought Stress. Plant Prod Sci 8:553–562.

871   65. Sebastian J, Yee M-C, Goudinho Viana W, Rellán-Álvarez R, Feldman M, Priest

872   HD, Trontin C, Lee T, Jiang H, Baxter I, Mockler TC, Hochholdinger F, Brutnell TP,

873   Dinneny JR. 2016. Grasses suppress shoot-borne roots to conserve water during

874   drought. Proc Natl Acad Sci U S A 113:8861–8866.

875   66. Wang Y, Schuck S, Wu J, Yang P, Döring A-C, Zeier J, Tsuda K. 2018. A MPK3/6-

876   WRKY33-ALD1-Pipecolic Acid Regulatory Loop Contributes to Systemic Acquired

877   Resistance. Plant Cell 30:2480–2494.

878   67. Hartmann M, Zeier J. 2019. N-hydroxypipecolic acid and salicylic acid: a metabolic

879   duo for systemic acquired resistance. Curr Opin Plant Biol 50:44–57.

880   68. Hartmann M, Zeier T, Bernsdorff F, Reichel-Deland V, Kim D, Hohmann M,

881   Scholten N, Schuck S, Bräutigam A, Hölzel T, Ganter C, Zeier J. 2018. Flavin

882   Monooxygenase-Generated N-Hydroxypipecolic Acid Is a Critical Element of Plant

883   Systemic Immunity. Cell 173:456–469.e16.

884   69. Cao H, Bowling SA, Gordon AS, Dong X. 1994. Characterization of an Arabidopsis

885   Mutant That Is Nonresponsive to Inducers of Systemic Acquired Resistance. Plant

886   Cell 6:1583–1592.

887   70. Jung HW, Tschaplinski TJ, Wang L, Glazebrook J, Greenberg JT. 2009. Priming in

888   systemic plant immunity. Science 324:89–91.

889   71. Wang C, El-Shetehy M, Shine MB, Yu K, Navarre D, Wendehenne D, Kachroo A,

890   Kachroo P. 2014. Free radicals mediate systemic acquired resistance. Cell Rep

891   7:348–355.

892   72. Henry A, Doucette W, Norton J, Bugbee B. 2007. Changes in crested wheatgrass

893   root exudation caused by flood, drought, and nutrient stress. J Environ Qual

894   36:904–912.

895   73. Preece C, Farré-Armengol G, Llusià J, Peñuelas J. 2018. Thirsty tree roots exude

896   more carbon. Tree Physiol 38:690–695.

897   74. You J, Zhang Y, Liu A, Li D, Wang X, Dossa K, Zhou R, Yu J, Zhang Y, Wang L,

898   Zhang X. 2019. Transcriptomic and metabolomic profiling of drought-tolerant and

899   susceptible sesame genotypes in response to drought stress. BMC Plant Biol

900   19:267.

901   75. Holmes EC, Chen Y-C, Sattely E, Mudgett MB. 2019. Conservation of N-hydroxy-

902   pipecolic acid-mediated systemic acquired resistance in crop plants. bioRxiv.

903   76. He Q, Zhao S, Ma Q, Zhang Y, Huang L, Li G, Hao L. 2014. Endogenous Salicylic

904   Acid Levels and Signaling Positively Regulate Arabidopsis Response to

905   Polyethylene Glycol-Simulated Drought Stress. J Plant Growth Regul 33:871–880.

906   77. La VH, Lee B-R, Islam MT, Park S-H, Jung H-I, Bae D-W, Kim T-H. 2019.

907   Characterization of salicylic acid-mediated modulation of the drought stress

908   responses: Reactive oxygen species, proline, and redox state in Brassica napus.

909   Environ Exp Bot 157:1–10.

910   78. Ding Y, Dommel M, Mou Z. 2016. Abscisic acid promotes proteasome-mediated

911   degradation of the transcription coactivator NPR 1 in Arabidopsis thaliana. Plant J

912   86:20–34.

913   79. Schnake A, Hartmann M, Schreiber S, Malik J, Brahmann L, Yildiz I, von Dahlen J,

914   Rose LE, Schaffrath U, Zeier J. 2020. Inducible biosynthesis and immune function

915   of the systemic acquired resistance inducer N-hydroxypipecolic acid in

916   monocotyledonous and dicotyledonous plants. J Exp Bot.

917   80. Gouesbet G, Blanco C, Hamelin J, Bernard T. 1992. Osmotic adjustment in

918   Brevibacterium ammoniagenes: pipecolic acid accumulation at elevated

919   osmolalities. J Gen Microbiol 138:959–965.

920   81. Gouesbet G, Jebbar M, Talibart R, Bernard T, Blanco C. 1994. Pipecolic acid is an

921   osmoprotectant for Escherichia coli taken up by the general osmoporters ProU and

922   ProP. Microbiology 140 (Pt 9):2415–2422.

923   82. Gouffi K, Bernard T, Blanco C. 2000. Osmoprotection by pipecolic acid in

924   Sinorhizobium meliloti: specific effects of D and L isomers. Appl Environ Microbiol

925   66:2358–2364.

926 83. Neshich IAP, Kiyota E, Arruda P. 2013. Genome-wide analysis of lysine catabolism

927   in bacteria reveals new connections with osmotic stress resistance. ISME J 7:2400–

928   2410.

929 84. Gao C, Montoya L, Xu L, Madera M, Hollingsworth J, Purdom E, Singan V, Vogel J,

930   Hutmacher RB, Dahlberg JA, Coleman-Derr D, Lemaux PG, Taylor JW. 2020.

931   Fungal community assembly in drought-stressed sorghum shows stochasticity,

932   selection, and universal ecological dynamics. Nat Commun 11:34.

933 85. Simmons T, Caddell DF, Deng S, Coleman-Derr D. 2018. Exploring the Root

934   Microbiome: Extracting Bacterial Community Data from the Soil, Rhizosphere, and

935   Root Endosphere. J Vis Exp.

936 86. Bolyen E, Rideout JR, Dillon MR, Bokulich NA, Abnet CC, Al-Ghalith GA, Alexander

937   H, Alm EJ, Arumugam M, Asnicar F, Bai Y, Bisanz JE, Bittinger K, Brejnrod A,

938   Brislawn CJ, Brown CT, Callahan BJ, Caraballo-Rodríguez AM, Chase J, Cope EK,

939   Da Silva R, Diener C, Dorrestein PC, Douglas GM, Durall DM, Duvallet C,

940   Edwardson CF, Ernst M, Estaki M, Fouquier J, Gauglitz JM, Gibbons SM, Gibson

941   DL, Gonzalez A, Gorlick K, Guo J, Hillmann B, Holmes S, Holste H, Huttenhower C,

942   Huttley GA, Janssen S, Jarmusch AK, Jiang L, Kaehler BD, Kang KB, Keefe CR,

943   Keim P, Kelley ST, Knights D, Koester I, Kosciolek T, Kreps J, Langille MGI, Lee J,

944   Ley R, Liu Y-X, Loftfield E, Lozupone C, Maher M, Marotz C, Martin BD, McDonald

945   D, McIver LJ, Melnik AV, Metcalf JL, Morgan SC, Morton JT, Naimey AT, Navas-

946   Molina JA, Nothias LF, Orchanian SB, Pearson T, Peoples SL, Petras D, Preuss

947   ML, Pruesse E, Rasmussen LB, Rivers A, Robeson MS 2nd, Rosenthal P, Segata

948   N, Shaffer M, Shiffer A, Sinha R, Song SJ, Spear JR, Swafford AD, Thompson LR,

949   Torres PJ, Trinh P, Tripathi A, Turnbaugh PJ, Ul-Hasan S, van der Hooft JJJ,

950   Vargas F, Vázquez-Baeza Y, Vogtmann E, von Hippel M, Walters W, Wan Y, Wang

951   M, Warren J, Weber KC, Williamson CHD, Willis AD, Xu ZZ, Zaneveld JR, Zhang Y,

952   Zhu Q, Knight R, Caporaso JG. 2019. Reproducible, interactive, scalable and

953   extensible microbiome data science using QIIME 2. Nat Biotechnol 37:852–857.

954 87. Callahan BJ, McMurdie PJ, Rosen MJ, Han AW, Johnson AJA, Holmes SP. 2016.

955   DADA2: High-resolution sample inference from Illumina amplicon data. Nat

956   Methods 13:581–583.

957 88. Development Core Team RR. 2011. R: A language and environment for statistical

958   computing.

959 89. McMurdie PJ, Holmes S. 2013. phyloseq: an R package for reproducible interactive

960   analysis and graphics of microbiome census data. PLoS One 8:e61217.

961 90. Dixon P. 2003. VEGAN, a package of R functions for community ecology. J Veg Sci

962   14:927–930.

963 91. Yao Y, Sun T, Wang T, Ruebel O, Northen T, Bowen BP. 2015. Analysis of

964   Metabolomics Datasets with High-Performance Computing and Metabolite Atlases.

965   Metabolites 5:431–442.

966 92. Smith CA, O'Maille G, Want EJ, Qin C, Trauger SA, Brandon TR, Custodio DE,

967   Abagyan R, Siuzdak G. 2005. METLIN: a metabolite mass spectral database. Ther

968   Drug Monit 27:747–751.

969   93. Oliveros JC. 2016. Venny. An interactive tool for comparing lists with Venn's

970   diagrams. 2007--2015.

971   94. Chong J, Soufan O, Li C, Caraus I, Li S, Bourque G, Wishart DS, Xia J. 2018.

972   MetaboAnalyst 4.0: towards more transparent and integrative metabolomics

973   analysis. Nucleic Acids Res 46:W486–W494.

974   95. Chong J, Wishart DS, Xia J. 2019. Using MetaboAnalyst 4.0 for Comprehensive

975   and Integrative Metabolomics Data Analysis. Curr Protoc Bioinformatics 68:e86.

976   96. Mishina TE, Zeier J. 2006. The Arabidopsis flavin-dependent monooxygenase

977   FMO1 is an essential component of biologically induced systemic acquired

978   resistance. Plant Physiol 141:1666–1675.

979   97. Cao H, Glazebrook J, Clarke JD, Volko S, Dong X. 1997. The Arabidopsis NPR1

980   gene that controls systemic acquired resistance encodes a novel protein containing

981   ankyrin repeats. Cell 88:57–63.

982   98. Torres MA, Dangl JL, Jones JDG. 2002. Arabidopsis gp91phox homologues

983   AtrbohD and AtrbohF are required for accumulation of reactive oxygen

984   intermediates in the plant defense response. Proc Natl Acad Sci U S A 99:517–522.

985   99. Lamesch P, Berardini TZ, Li D, Swarbreck D, Wilks C, Sasidharan R, Muller R,

986   Dreher K, Alexander DL, Garcia-Hernandez M, Karthikeyan AS, Lee CH, Nelson

987   WD, Ploetz L, Singh S, Wensel A, Huala E. 2012. The Arabidopsis Information

988   Resource (TAIR): improved gene annotation and new tools. Nucleic Acids Res

989   40:D1202–10.

990 100.   Schneider CA, Rasband WS, Eliceiri KW. 2012. NIH Image to ImageJ: 25 years

991   of image analysis. Nat Methods 9:671–675.

992 **Tables**

993 Table 1. Detailed information on significantly changed metabolites between drought and

994 watered roots

Proposed metabolite	Molecular formula	Measured m/z	ppm error	Measured RT peak (minutes)	RT error	MSMS quality score*	Ion mode	Log2 (FC)	p-value (root)	q-value (root)	Significant compartment(s)**
methionine	C5H11NO2S	148.044	1.748	10.6	0.1	1	negative	3.21	0.001	0.016	RZS
proline	C5H9NO2	116.071	2.444	11.1	0.1	1	positive	2.82	0.001	0.016	RZS
betaine	C5H12NO2+	118.087	2.456	7.8	0.2	1	positive	2.48	0.000	0.016	RZS
carnitine	C7H16NO3+	162.113	0.503	13.2	0.2	1	positive	2.43	0.012	0.038	RZS
N-trimethyllysine	C9H21N2O2+	189.160	0.178	16.8	0.1	1	positive	5.49	0.002	0.020	RZ
3-hydroxykynurenine	C10H12N2O4	225.087	0.497	11.2	0.1	0	positive	4.54	0.012	0.038	RZ
lysine	C6H14N2O2	147.113	0.569	17.0	0.1	1	positive	4.24	0.001	0.016	RZ
taurine	C2H7NO3S	126.022	1.176	12.3	0.0	0	positive	3.94	0.012	0.038	RZ
arginine	C6H14N4O2	175.119	0.691	17.0	0.1	1	positive	3.81	0.002	0.018	RZ
pipecolic acid	C6H11NO2	130.086	0.888	11.0	0.0	1	positive	3.39	0.001	0.016	RZ
allothreonine// homoserine// threonine	C4H9NO3	120.066	1.912	13.7	0.1	0	positive	3.25	0.003	0.021	RZ
valine	C5H11NO2	116.072	1.809	11.2	0.0	1	negative	3.15	0.003	0.020	RZ
1-aminocyclopropane-1-carboxylic acid	C4H7NO2	102.055	3.955	13.7	0.6	1	positive	3.14	0.003	0.020	RZ
2-amino-2-methylpropanoic acid	C4H9NO2	104.071	4.409	12.5	0.0	1	positive	2.98	0.004	0.025	RZ
asparagine	C4H8N2O3	133.061	0.814	14.5	0.1	1	positive	2.91	0.006	0.027	RZ
cis-4-hydroxy-proline//trans-4-hydroxyproline	C5H9NO3	130.051	0.823	13.4	0.3	0	negative	2.90	0.004	0.022	RZ
guanidinoacetic acid	C3H7N3O2	118.061	2.161	14.0	0.1	0	positive	2.43	0.003	0.020	RZ
deoxycarnitine	C7H16NO2+	146.118	0.662	13.3	0.2	1	positive	2.39	0.024	0.061	RZ
serotonin	C10H12N2O	177.102	0.870	8.7	0.1	0	positive	3.47	0.042	0.087	RO
histidinol	C6H11N3O	142.098	0.107	12.9	0.2	0	positive	2.95	0.014	0.044	RO
trans-4-hydroxyproline	C5H9NO3	132.066	0.768	13.4	0.1	0	positive	2.83	0.004	0.022	RO
o-acetyl-serine	C5H9NO4	148.060	0.072	11.4	0.1	-1	positive	2.83	0.016	0.045	RO
4-methoxyphenylacetic acid	C9H10O3	184.097	0.912	1.1	0.0	0	positive	2.79	0.005	0.026	RO
riboflavin	C17H20N4O6	377.146	1.147	4.6	0.0	0	positive	2.67	0.004	0.025	RO
hippuric acid	C9H9NO3	180.066	0.924	4.6	0.3	0	positive	2.41	0.009	0.034	RO
acetylcholine	C7H16NO2+	146.118	0.496	2.1	0.1	1	positive	2.38	0.010	0.036	RO
pyridoxamine	C8H12N2O2	169.097	0.267	10.2	0.0	0	positive	2.12	0.001	0.016	RO
abscisic acid	C15H20O4	247.133	1.332	1.1	0.0	0	positive	2.05	0.006	0.026	RO
2,3-dihydroxybenzoic acid// 2,5-dihydroxybenzoic acid// 3,4-dihydroxybenzoic acid	C7H6O4	153.020	1.467	4.0	0.1	0	negative	-2.11	0.000	0.012	RO
xylitol	C5H12O5	175.058	4.087	5.1	0.0	0	positive	-3.16	0.001	0.016	RO
4-methylcatechol	C7H8O2	123.045	1.158	4.3	0.4	0	negative	-3.73	0.001	0.016	RO

*MSMS quality scores: 1 (MSMS matches ref. std.); 0.5 (possible match); 0 (no MSMS collected or no appropriate ref available); -1 (MSMS poor match to ref. std.)

995 **Compartment(s) with significant Log2 (fold change): Root, rhizosphere, and soil (RZS); root and rhizosphere (RZ); root only (RO)

996

997 Table 2. Detailed information on significantly changed metabolites 24 hours after

998 rewatering

Proposed metabolite	Molecular formula	Measured *m/z*	ppm error	Measured RT peak (minutes)	RT error	MSMS quality score*	Ion mode	Log2 (FC)	p-value (root)	q-value (root)	Significant compartment
4-imidazoleacetic acid	C5H6N2O2	127.050	0.936	13.9	0.2	1	positive	-2.44	0.049	0.296	rhizosphere
1-aminocyclopropane-1-carboxylic acid	C4H7NO2	102.055	3.955	13.7	0.6	1	positive	-2.44	0.047	0.296	rhizosphere
pipecolic acid	C6H11NO2	130.086	0.888	11.0	0.0	1	positive	-2.45	0.048	0.296	rhizosphere
carnitine	C7H16NO3+	162.113	0.503	13.2	0.2	1	positive	-2.49	0.017	0.231	rhizosphere
melatonin	C13H16N2O2	233.128	1.296	1.2	0.0	0	positive	-2.89	0.011	0.213	rhizosphere
3-hydroxyanthranilic acid	C7H7NO3	152.036	1.229	1.8	0.1	0	negative	-3.11	0.003	0.135	rhizosphere
syringic acid	C9H10O5	197.046	0.404	1.6	0.1	1	negative	-3.42	0.040	0.296	rhizosphere
cytidine 2',3'-cyclic mono-phosphoric acid	C9H12N3O7P	306.049	1.863	14.0	0.2	0	positive	-3.44	0.047	0.296	rhizosphere
abscisic acid	C15H20O4	247.133	1.332	1.1	0.0	0	positive	-3.56	0.002	0.135	rhizosphere
galactitol//mannitol	C6H14O6	181.072	1.680	9.7	0.1	1	negative	-3.58	0.026	0.263	rhizosphere
4-methylcatechol	C7H8O2	123.045	1.158	4.3	0.4	0	negative	-4.45	0.005	0.169	rhizosphere
2,3-dihydroxybenzoic acid//2,5-dihydroxybenzoic acid//3,4-dihydroxybenzoic acid	C7H6O4	153.020	1.467	4.0	0.1	0	negative	-4.45	0.040	0.296	rhizosphere
erythritol	C4H10O4	121.051	0.626	3.2	0.0	1	negative	-5.04	0.024	0.252	rhizosphere
arabitol	C5H12O5	151.061	1.358	5.6	0.2	1	negative	-5.29	0.003	0.135	rhizosphere
sn-glycero-3-phosphocholine	C8H21NO6P+	258.110	0.111	14.8	0.2	1	positive	-5.66	0.017	0.231	rhizosphere
guanosine 3',5'-cyclic monophosphoric acid	C10H12N5O7P	346.055	0.947	13.9	0.2	0	positive	-5.73	0.000	0.019	rhizosphere
ferulic acid	C10H10O4	193.051	0.614	1.3	0.1	1	negative	-5.75	0.008	0.181	rhizosphere
lactose//trehalose	C12H22O11	401.131	1.143	14.4	0.1	1	negative	-3.07	0.002	0.340	soil

*MSMS quality scores: 1 (MSMS matches ref. std.); 0.5 (possible match); 0 (no MSMS collected or no appropriate ref available); -1 (MSMS poor match to ref. std.)

999

1000

1001   **Figure captions**

1002

1003   **Figure 1. Sorghum root-associated microbiome responds to drought and**

1004   **rewatering. A** Representative image of sorghum plants following eight weeks of a

1005   preflowering drought (TP8). **B** Phylum level relative abundances of sorghum root,

1006   rhizosphere, and soil microbiomes at TP8 and 24 hours after rewatering (24h DW) in

1007   well-watered (W) or drought (D) plots. **C** Alpha diversity (Shannon) of sorghum root,

1008   rhizosphere, and soil. **D** Beta diversity (PCoA) of sorghum root, rhizosphere, and soil

1009   microbiomes at TP8 and 24 hours after rewatering in well-watered control or drought

1010   plots. **E-J** Relative abundances of individual lineages that displayed a significant

1011   difference in abundance between watering treatments (ANOVA, Tukey-HSD, $P<0.05$).

1012

1013   **Figure 2. Metabolic profiles during drought differ by compartment. A** Heatmap of

1014   relative peak heights of all observed metabolites (n=168) across root, rhizosphere

1015   (rhizo), and soil compartments and watered (W) and drought (D) treatments. **B** Principal

1016   component analysis (PCA) plot of root, rhizosphere, and soil metabolites. **C**

1017   Proportional Venn diagram of drought enriched metabolites in root, rhizosphere, or soil

1018   (D/W Log_2 fold change >2, t-test p<0.05). **D-E** Heatmap of the subset of metabolites

1019   that were enriched or depleted in roots during drought, with the predicted identity of

1020   metabolites listed beside each row.

1021

1022   **Figure 3. Rewatering depletes rhizosphere metabolites following a prolonged**

1023   **drought. A** Heatmap of relative peak heights of all observed metabolites (n=168)

1024 across three compartments (root, rhizosphere (rhizo), and soil), three treatments

1025 (watered (W), drought (D), drought rewatered (DW), and two time points (time point 8

1026 (TP8) and 24 hours later (24h)). **B-C** Heatmap of the subset of metabolites that were

1027 depleted after rewatering (DW/D Log$_2$ fold change < -2, t-test p<0.05), with the

1028 predicted identity of metabolites listed beside each row. Note, all significant depletions

1029 were observed in the rhizosphere, except trehalose, which occurred in soil. **D** Principal

1030 component analysis (PCA) plot of root, rhizosphere, and soil metabolites.

1031

1032 **Figure 4. Pipecolic acid abundance pattern mirrors drought markers. A** The top 10

1033 metabolites correlated with the drought marker betaine across all sample types,

1034 treatments, and time points. **B-D** Log$_{10}$ peak heights of individual metabolites. Each

1035 point represents an individual sample of root (green), rhizosphere (blue), or soil (yellow).

1036 Dashed lines represent the limit of detection for individual metabolites, based on the

1037 average log$_{10}$ peak heights of the sample blanks for root (red) or rhizosphere and soil

1038 (blue). **E** Heatmap of relative abundance of all metabolites and bacteria ASVs (grouped

1039 at the class level), clustered within the root, across treatments (watered (W), drought

1040 (D), drought rewatered (DW), and time points (time point 8 (TP8) and 24 hours later

1041 (24h)). **F** Zoom-in of Actinobacteria and closely clustering root metabolites, as

1042 highlighted in pink in figure 4e. Actinobacteria and the metabolites that are closely

1043 correlated with betaine (as in figure 4a) are in bold.

1044

1045 **Figure 5. Pipecolic acid reduces root growth. A** Root lengths of sterilized sorghum

1046 seedlings after 7 days of growth in water containing 0, 0.1, or 1 mM pipecolic acid (Pip).

1047   Different letters indicate a significant difference in root length (ANOVA, Tukey-HSD,

1048   p<0.05). This experiment was performed twice with similar results. **B** Two

1049   representative seedlings from each treatment were photographed at the time of

1050   measurement. **C** Root lengths of sterilized Arabidopsis seedlings after 10 days of

1051   growth in ½ MS+ 1% sucrose agar media containing 0, 0.001, 0.01, 0.1, or 1 mM Pip.

1052   Different letters indicate a significant difference in root length (ANOVA, Tukey-HSD,

1053   p<0.05). Different colors represent plants from independent experiments (n=3). **D** One

1054   representative plate from 0 and 1 mM pipecolic acid treatments were photographed at

1055   the time of measurement.

1056

1057   **Figure 6. Pipecolic acid root growth reduction is SAR-independent. A** Root length

1058   of Arabidopsis Col-0 (WT) and Arabidopsis mutants grown on 1/2MS + 1% sucrose

1059   plates containing 0 or 1 mM Pip. Significance between treatments was evaluated by

1060   ANOVA with Tukey's HSD posthoc test (p<0.05). Different colors represent plants from

1061   independent experiments. **B** Simplified SAR pathway. Highlighted in red are the

1062   Arabidopsis mutants used to evaluate a potential interaction between SAR and Pip-

1063   mediated root growth suppression.